Corrosion Science 87 (2014) 1–5

Contents lists available at ScienceDirect

Corrosion Science

journal homepage: www.elsevier.com/locate/corsci

Letter

Effects of inclusions on the precipitation of chi phases and intergranular corrosion resistance of hyper duplex stainless steel

Soon-Hyeok Jeon, Hye-Jin Kim, Yong-Soo Park *

Department of Material Science and Engineering, Yonsei University, 134 Shinchon-dong, Seodaemun-gu, Seoul 120-749, Republic of Korea

ARTICLE INFO

Article history:
Received 19 May 2014
Accepted 4 June 2014
Available online 13 June 2014

Keywords:
A. Stainless steel
B. EPMA
C. Inclusion
C. Intergranular corrosion

ABSTRACT

During the initial stage of aging heat treatment at 850 °C, inclusions such as (Cr, Mn, Al) oxides and (Cr, Mn, Al, Fe) oxides of a hyper duplex stainless steel act as preferential precipitation sites for the chi phase like ferrite/austenite phase boundaries and ferrite/ferrite grain boundaries. The chi phase is precipitated around the inclusions due to the blocking and piling up the alloying elements such as Mo and W around the inclusions. The precipitation of Mo and W enriched chi phase around the inclusions decreases the intergranular corrosion resistance due to the formation of Mo and W depleted zones.

1. Introduction

Super duplex stainless steels (SDSSs) consisting of ferrite (α) and austenite (γ) phases are increasingly being used in various applications, including in power plants, desalination facilities, and marine construction due to their excellent mechanical properties and corrosion resistance. [1–3]. Recently, when used in heat exchangers, SDSSs exhibit the corrosion resistance that is insufficient to allow for high temperature operations and a long service life. Hence, highly alloyed hyper duplex stainless steel (HDSSs), which exhibit high corrosion resistance, combined with improved mechanical properties, have been developed.

However, duplex stainless steels (DSSs) formed undesired secondary phases such as the sigma (σ) and chi (χ) phases at 700–950 °C during hot rolling or welding [4–6]. The secondary phases degraded the corrosion resistance and the mechanical properties of the steels due to their inherent brittleness and the formation of Cr, Mo, and W depleted regions around the secondary phases [7–12].

The effects of various alloying elements on the precipitation of secondary phases such as the σ and χ phases have been investigated previously. The addition of N reduces the tendency of the σ phase formation in the α phase since it results in the removal of Cr from the solution through the formation of chromium nitride [13]. The addition of C in ferritic stainless steels (FSSs) retards the formation of the σ phase by increasing the incubation period [14]. The addition of a small amount of Ce (55–110 ppm) to the HDSSs results in the homogeneous distribution of Ce in the alloy matrix and delays the precipitation of the secondary phases by reducing the diffusion rates of Cr, Mo, and W [15]. The addition of Cu to the HDSSs facilitates the precipitation rate of the χ phase due to the increase in the activity of W and retards the precipitation of the σ phase due to the decrease in the activity of Mo [16]. Partial substitution of W for Mo retarded the precipitation of the σ phase in the HDSSs. This was due to an increase in the tendency of formation of the χ phase with a higher nucleation efficiency and lower growth rate than those of the σ phase [17].

There have been a few reports suggesting that the precipitation of secondary phases such as the σ and χ phases can be retarded by increasing the grain size of the α phase and α grains act as preferential precipitation sites for the secondary phases in the DSSs [18]. In addition, the σ phase precipitation in the DSSs is affected by the crystallographic orientation relationship at the α/γ interface, and highly coherent and low-energy α/γ interfaces can effectively suppress the precipitation [19].

Meanwhile, the effects of the inclusion on the pitting corrosion have been investigated. Pit initiation occurred as a result of crevice formation between the inclusion and metallic matrix. The inclusions dominate as pit nucleation sites, and the lifetime of a metastable pit is directly related to the size of the inclusion particle [20]. Suter and Böhni [21] showed that pit nuclei originating from small inclusions (<1 μm) were hardly transformed into steadily growing pits. The pitting potentials depended on the size of the largest inclusions present in the stainless steel [22].

It is well known that the metastable pits as a precursor state to the stable pits form at potentials far below the pitting potential of stainless steels [23–27]. The metastable pitting, which involves the

* Corresponding author. Tel.: +82 2 2123 2836; fax: +82 2 362 9199.
E-mail addresses: junsoon@yonsei.ac.kr (S.-H. Jeon), corrus@yonsei.ac.kr (Y.-S. Park).

http://dx.doi.org/10.1016/j.corsci.2014.06.019
0010-938X/

pit nucleation, possible propagation and termination, occurs through the local breakdown of the passivating oxide film. The growth of the metastable pit is a well-documented feature of the pitting corrosion of stainless steels in chloride solutions [28,29]. Burstein suggested that there are two distinct processes that precede the stable pit formation: pit nucleation and growth of the metastable pit [30,31].

So far, many investigations have been made on the effects of the inclusions on the pitting corrosion resistance and metastable pit of stainless steels. However, the detailed role of the inclusions on the precipitation of deleterious χ phase and associated intergranular corrosion resistance during the initial stage of aging heat treatment has not yet been investigated.

In this study, to elucidate the effects of the inclusions on the precipitation of the χ phase and the intergranular corrosion resistance of the HDSS alloy, a double-loop electrochemical potentiokinetic reactivation (DL-EPR) test, a scanning electron microscope–energy dispersive X-ray spectroscopy (SEM–EDS) analysis and an electron probe micro-analyzer (EPMA) analysis were performed.

2. Experimental procedures

Ingots weighing 50 kg with dimensions 150 by 150 by 300 mm (width by length by height) were manufactured using a high frequency vacuum induction furnace. After these ingots were hot rolled in the range of 1050–1250 °C, plates of 6 mm thickness were manufactured. The chemical composition of the alloy is presented in Table 1. The experimental alloy was cut and solution heat-treated for 5 min per 1 mm thickness at 1090 °C and then quenched in water. The specimen was then isothermally aged at 850 °C for 10 min. To observe the microstructures of the HDSS alloy, it was ground to 2000 grit using silicon carbide (SiC) abrasive papers, polished surface using diamond paste. The sample was ultrasonic cleaned in acetone and distilled water to remove any impurities from the polished surface of the sample. The χ phases and chromium nitrides were observed using SEM in backscattered electron mode (BSE). In addition, the chemical compositions of the χ phases and chromium nitrides were analyzed by the EDS attached to the SEM. The line profiles of the Cr, Mo and W in the χ phase around inclusions were measured using the EPMA.

Table 1
Chemical composition of the experimental alloy (wt.%).

Alloy	C	Cr	Ni	Mo	W	Si	Mn	N	S	Fe
HDSS	0.02	27.01	7.00	2.52	3.28	0.35	0.88	0.35	0.003	Bal.

The DL-EPR tests are conducted following the recommendations of Majidi and Streicher [32]. The DL-EPR test was originally used to evaluate the degree of sensitization (DOS) of stainless steels [33]. The DL-EPR test was applied to selectively attack the matrix around fine precipitates formed during aging, without the attack on the precipitates themselves. The DL-EPR test was carried out using an EG&G PAR 263A potentiostat model. The standard test solution (0.5 M sulfuric acid (H_2SO_4) + 0.01 M potassium thiocyanate (KSCN)) was used for austenite stainless steels (ASSs). On the other hand, a more aggressive solution (2 M H_2SO_4 + 0.01 M KSCN + 0.5 M sodium chloride (NaCl)) was used for the DSSs with more excellent corrosion resistance than ASSs [34]. The DL-EPR test was conducted in 2 M H_2SO_4 + 0.01 M KSCN + 0.5 M NaCl solution at 30 °C. The DOS of the experimental alloy was evaluated by measuring the ratio of reactivation peak current (i_r) to activation peak current (i_a) when the potential was applied at a scan rate of 0.06 V/min from −600 to 200 mV_{SCE}, and then reversely to −600 mV_{SCE}, respectively.

3. Results and discussion

Fig. 1 shows the SEM–BSE images of the solution-annealed HDSS alloy specimen and aged HDSS alloy at 850 °C for 10 min. The solution-annealed alloy specimen had the γ phase and α phase without secondary phases. The γ phase can be seen as an isolated phase on the background of the α phase, which looks relatively dark. As presented in Fig. 1(a), the chemical compositions and the morphologies of the inclusions of the black spots were analyzed using the SEM–EDS analyses. The inclusions in the HDSS alloy were composed of the main type of the (Cr, Mn, Al) oxides and (Cr, Mn, Fe, Al) oxides.

Meanwhile, after the specimen had being aged at 850 °C for 10 min, it was found that the precipitates were formed in the specimen and that these precipitates formed continuous networks along the grain boundaries as well as randomly within the grains (Fig. 1(b)). These precipitates were the χ phase and chromium nitrides and chemical compositions of these were confirmed by the SEM–EDS analyses. The only precipitates larger than size of 1 μm were selected in order to minimize the influence of the matrix on the analysis results. A few precipitates of the χ phases continuously formed along the phase boundaries between the γ and α phases in the alloy. The χ phase grew further along the phase boundaries between γ and α phases and within the α grains. It is known that the χ phases nucleate at the α/γ phase boundaries and within the α grains [16–18]. In general, the secondary phase forms more easily in high-energy regions, such as at the α/γ interfaces, through a heterogeneous nucleation process [35]. During the initial stage of aging heat treatment at 850 °C, the inclusions such

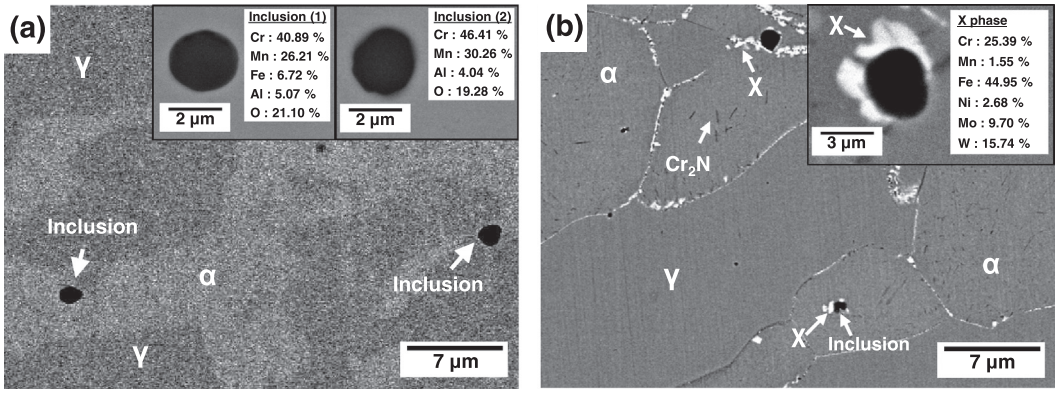

Fig. 1. SEM–BSE images of the HDSS alloy: (a) the solution annealed specimen at 1090 °C for 30 min and (b) the aged specimen at 850 °C for 10 min.